IOP Conf. Series: Materials Science and Engineering **181** (2017) 012023 doi:10.1088/1757-899X/181/1/012023

Experimental and numerical investigation of the residual yield strength of aluminium alloy EN AW-2024-T3 affected by artificially produced pitting corrosion

R Pippig[1], E Schmidl[1], P Steinert[2], A Schubert[2] and T Lampke[1]

[1]Institute of Materials Science and Engineering, Chemnitz University of Technology, 09125 Chemnitz, Germany
[2]Professorship Micromanufacturing Technology, Institute for Machine Tools and Production Processes, Chemnitz University of Technology, 09126 Chemnitz, Germany

Abstract. In this study, the behaviour of the residual yield strength of aluminium alloy EN AW-2024-T3 affected by the morphology and numbers of corrosion pits (defects) is presented. Since specific defect structures are not reproducible during experimental corrosion tests, metal sheets with different numbers of pits and pit shapes are produced using laser micro structuring. The defect structures are measured using laser scanning microscopy. To compare the stress states of the micro structured and real corroded metal sheets, FE-analysis is used. Afterwards, uniaxial tensile tests are carried out and critical defect parameters in terms of yield strength reduction of the investigated aluminium alloy are detected.

1. Introduction

High strength aluminium alloys are susceptive to local corrosion phenomena, especially pitting corrosion [1]. The susceptibility to local corrosion is caused by damage of the passive layer, e.g. by chloride ions [2, 3]. When the passive layer is destroyed, the propagation of the local corrosion begins. The process is accelerated by local differences in electrochemical potentials caused by precipitates [1, 4, 5]. As a result, deep penetrating pits grow from the surface into the bulk material. This pitting corrosion leads to a loss in mechanical properties due to a reduced cross section, local dealloying [6] and notch stresses [7, 8].

High-strength aluminium alloys are widely used in the automotive and aircraft industry, where the most components are stressed by oscillating forces. Hence, common research focuses on the impact of pitting corrosion on the fatigue strength [9-11]. But also the static behaviour of high-strength aluminium alloys damaged by pitting corrosion is a subject of present investigations [12-15]. Pantelakis et al. showed a significant decrease in yield strength of the aluminium alloy EN AW 2024-T3 after being exposed to the so called EXCO test [13, 15] and a 3.5% NaCl solution [13]. In further investigations Setsika et al. [14] used finite element simulations (FE) to calculate this decrease of yield strength. Thereby, they approximate the complex local corrosion damage with conical frustums. The geometry of the frustums is obtained from corrosion damage obtained from metallographic specimens [15].

In order to apply the founded correlations to component parts in service, the pit shape should be determined by a non-destructive method. For modelling the strength loss, the geometry of the pits should be preferred to the corrosion duration. The same corrosion parameters, e.g. exposure time,

result in different degrees of corrosion damage. Due to this reason it is not possible to achieve samples with equal damage by corrosion experiments in order to test parallel samples.

The aim of this work is to correlate the geometry and amount of corrosion damage (shape of pits, approximated by defect parameters) to the resulting quasi-static yield strength of the aluminium alloy EN AW 2024-T3. The natural pitting corrosion damage was imitated by artificial pits produced by laser micromachining. Metallographic and numerical results verify the suitability of this method. Using this approach, specimens with artificial pits varying in geometry and numbers are produced and uniaxial, quasi-static tensile tests are carried out to determine the residual yield strength.

2. Experimental procedure

The experiments were carried out using standard commercial aluminium alloy EN AW-2024-T3 sheets with dimensions of 100 x 25 x 1.6 mm³ (rolling direction (RD) parallel to the specimen length). All specimens were grinded along the transversal direction (TD) using 1000 mesh sizing SiC paper to achieve a uniform and comparable surface condition over all samples.

To recreate real pitting corrosion caused by electrochemical corrosion, laser micromachining was used. Therefore, defects with different machining parameters were generated on the surface of a metal sheet using a ND:YVO_4 laser by Spectra-Physics. Afterwards, the artificial defects were scanned using laser scanning microscopy (Keyence VK-X200) and metallographic cuttings were recorded to identify the best set of machining parameters, see table 1, in terms of reproducing real pitting corrosion. The metallographic cuttings were prepared using SiC grinding paper with a mesh size of 600, 1000, 2400 and 4000. After grinding, the samples were polished using diamond paste with a grain size of 3 µm and finally OPS-suspension. To quantify the morphology of pitting corrosion based on laser scanning microscopy (LSM), three parameters of a pit were defined. These are the maximal depth z, the width in RD x and the width in TD y. The widths x and y are measured through the coordinates of the maximal depth in RD and TD, respectively.

Beside the optical measurements, microhardness measurements (KB 250 BVRZ) around the artificial pits were performed to observe unexpected changes in the microstructure caused by the laser beam. Five measurements per area of interest were done.

Table 1. Set of layer machining parameters to produce the artificial pits.

Parameter	Value
Wave length	532 nm
Pulse duration	10 ns
Focus diameter	15 µm
Mean power	10.4 W
Pulse repetition frequency	150 kHz
Pulse and line distance	8 µm

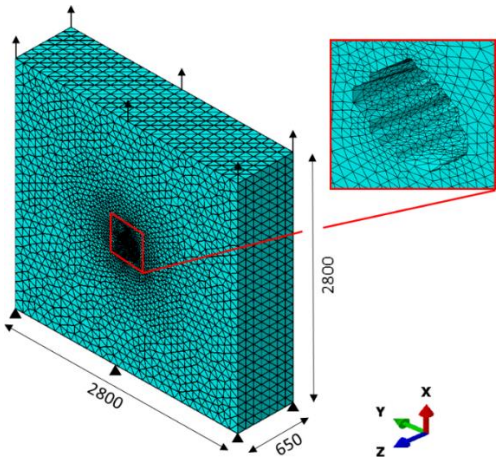

Figure 1. Geometry and mesh refinement for the FE-Analysis of a real corroded pit.

To compare the stress distributions induced by real corroded and artificial pits, the finite element analysis is used. Therefore, 3D profiles of the individual pits were measured using laser scanning microscopy and imported into the 3D surface modeller software Rhinozeros to create a solid CAD model. The pits were scaled to a size of 350 µm in x- and y-direction and a depth of 230 µm. Around the pits, a large enough solid block is defined to prevent interactions between the stress field of a pit

and the boundaries of the simulation area, see figure 1. In the literature the shape of the pits are often approximated using simple geometries, e.g. ellipsoids [16, 17] or conical frustums [14]. Therefore, the stress distribution around a conical frustum is also analysed and compared to the other pit structures. To calculate the stress distributions around the pits, one side of the block is fixed in *x*-direction and a load of 100 MPa is applied on the other side, see figure 1. The material is isotropic with a Young's Modulus of 77.4 GPa, a Possion's ratio of 0.33 and a density of 2.78 g/cm³. The plastic material behaviour is modelled using the experimental measured stress strain curve of the aluminium alloy EN AW 2024-T3 without pitting corrosion. The mesh size around and within the pits was refined until constant stress distributions were noted, see figure 1. All FE simulations were performed using the dynamic implicit solver with a quasi-static strain rate of 10^{-3} s^{-1}.

In order to determine the quasi-static strength of the alloy damaged by pitting, an unstandardized tensile specimen was used. The alternating dimensions for the tensile specimen were necessary because of the dimensions of the metal sheets. The tensile specimens had a measuring length of 15 mm and a width of 4 mm and were taken parallel to RD. Afterwards, pits with different defect parameters were generated on each tensile specimen after statistical considerations using the machining parameters presented in table 1. In order to minimize the reduction of the cross section, no more than one defect was generated per cross section. After laser micromachining, the generated pits were measured using laser scanning microscopy and the corresponding defect parameters were calculated. At the end, uniaxial tensile tests at room temperature (295 K) and a constant strain rate of 10^{-3} s^{-1} were carried out using a ZWICK Allround-Line 20 kN testing machine.

3. Results and discussion

3.1 Comparison of the pit shapes

Figure 2 illustrates the cross section of a typical pit resulting from electrochemical corrosion, see figure 2 (a), and an artificially produced pit, see figure 2 (b). The geometrical shapes are very similar, including the rough topography at the bottom of the defects. However, the micro structured pits have a convex shape at the flanks of the defects and no undercuts which can be obtained in case of real pitting corrosion.

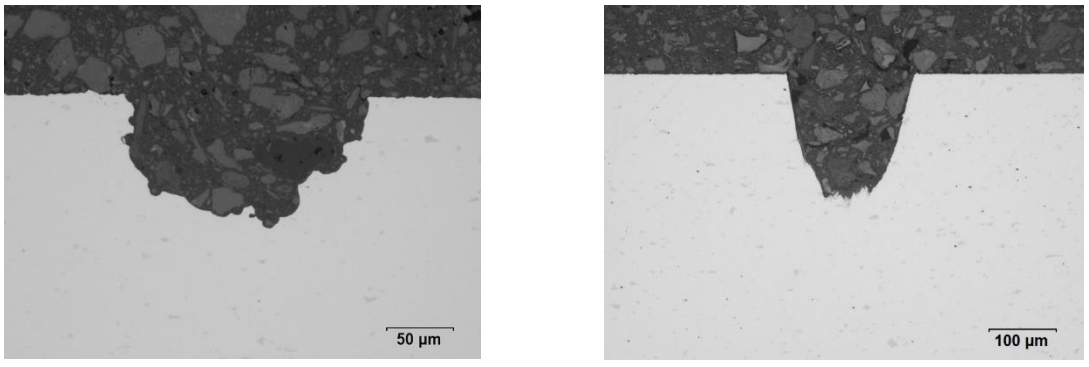

(a) (b)

Figure 2. Metallurgical specimens of a pit caused by (a) electrochemical corrosion (5 days salt spray test, 3.5 % NaCl, 40 °C) and (b) laser micromachining.

3.2 Comparison of hardness around the pits

Due to the laser beam, a heat impact into the material is seen when using laser microstructuring. This impact may result in microstructural changes of the heat treated aluminium alloy EN AW 2024-T3, influencing the microhardness and the yield strength, respectively. Therefore, the microhardness of the bulk material and the material around the pit were compared. For high-strength aluminium alloys, the hardness is usually measured in Brinell. However, because of the very limited space around the pits,

the microhardness measurements in Vickers hardness (HV) are more convenient for comparing the areas around the pits with the bulk material. The hardness of the bulk material is 162±8 HV 0.1 and the hardness around the area of the artificial pits is 151±11 HV 0.1, showing no significant differences. The fluctuations of the values are caused by the heterogeneous microstructure of the aluminium alloy, whereas changes in microstructure due to a heat treatment would result in much larger differences. An influence of the hardness caused by the laser could not be observed.

3.3 Numerical FE-Analysis of the stress distribution around the pits

In figure 3 (a), a representative overview over the total von Mises stresses inside and outside of the individual pits is shown. The stress distribution outside of a real corroded pit, see figure 3 (a), shows nearly zero stresses in tensile direction and maximum stresses of around 150 MPa perpendicular to it. This stresses are qualitatively and quantitatively comparable to the stresses outside of an artificially generated pit, see figure 3 (b), and even of a conical frustum pit, see figure 3 (c). In contrast to this, the stresses inside the conical frustum pit are totally different compared to the real and artificially generated defects. The maximum von Mises stress for the real corroded pit when applying a load of 100 MPa is 348.9 MPa, meanwhile the maximum stress of the conical frustum is 282.7 MPa (19.0 % lower). While the conical frustum pit shows a continuous decrease from the middle to the edge of the total von Mises stress in tensile direction, the stress inside of a real corroded pit is inhomogeneous due to its rough and rugged morphology. At the flanks of real pits, higher and lower stresses alternate from the middle to the edge in tensile direction. It can be assumed that due to the presented large stress state differences inside a simplified pit structure, the predicted strength behavior will depict insufficient results when using simple geometries.

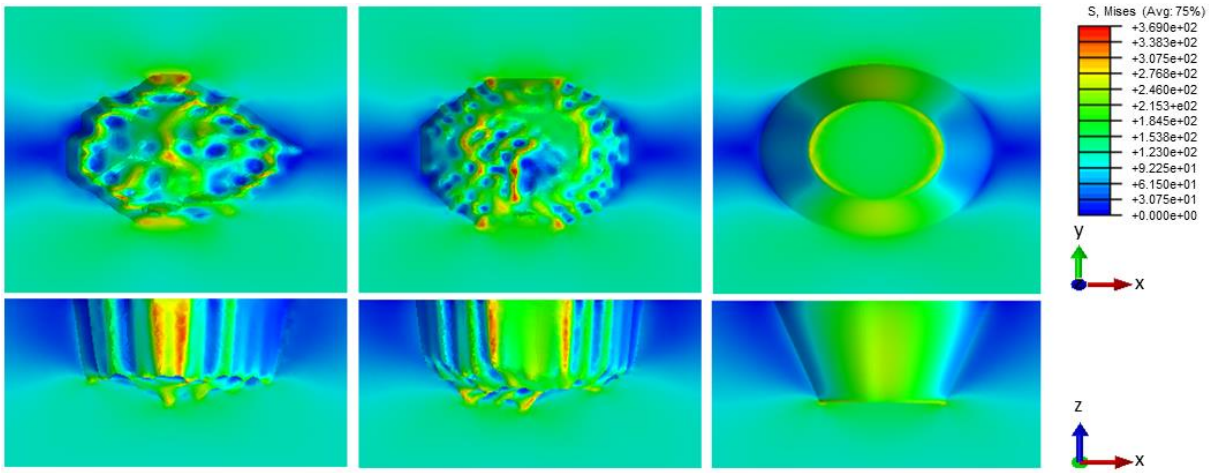

(a) (b) (c)

Figure 3. Numerical FE-Analysis of the total von Mises stress distribution around the (a) electrochemical corroded, (b) artificially generated and (c) conical frustum pit.

The artificially laser microstructured pits show a more accurate representation of real pits. The maximum von Mises stress with 368.3 MPa are only 5.6 % higher than the maximum stress of the representative real corroded pit. Also, the inhomogeneous stress distribution within the pit and the alternating stress profiles at the flanks of real pits is reproduced.

The finite element stress analysis as well as the experimental shape and hardness investigations show that micro laser machining is a sufficient method to imitate real corroded pits in terms of reproducing the strength behavior of the corroded aluminum alloy EN AW 2024-T3.

3.4 Mechanical properties

The influence of pitting on the mechanical properties in form of the yield strength reduction $\Delta R_{p0.2}$ is presented in figure 4. The relatively large standard deviations in yield strength between some parallel samples, see the bars in figure 4, are caused by the slightly different defect parameters of these samples. Especially, the pit depths can vary up to 21 µm because of the heterogeneous microstructure due to the precipitations within the aluminum matrix. This leads to a different amount of material removal during the laser micro machining process, resulting in slightly different depths and widths of the pits.

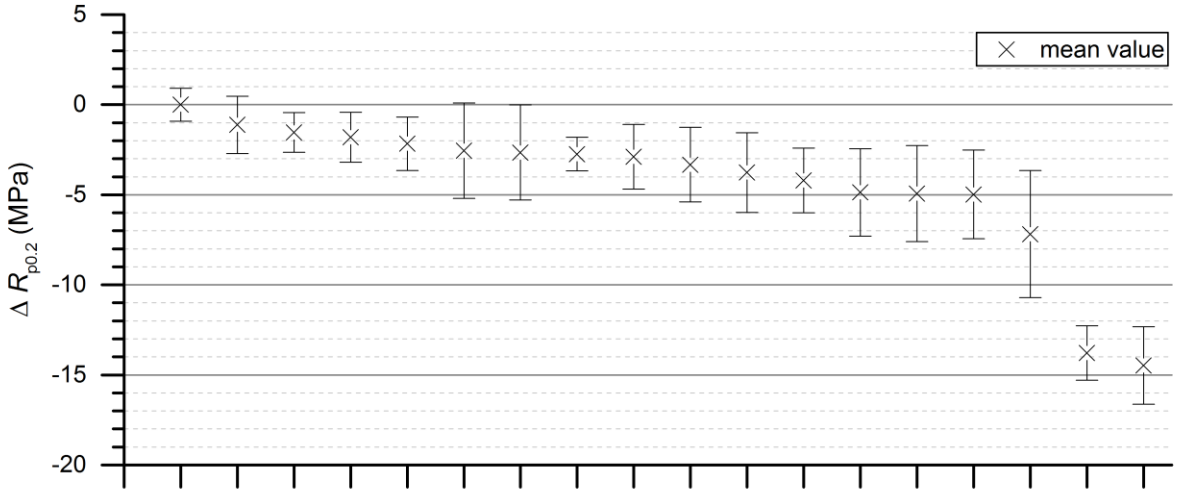

z (µm)	0	188±12	133±12	83±6	130±13	89±4	261±6	164±7	75±14	252±1	56±11	274±18	301±2	253±4	95±4	296±21	291±19	225±9
x (µm)	0	194±7	138±8	110±6	131±10	85±4	236±21	244±2	47±5	353±1	49±8	242±16	341±4	336±8	139±6	433±7	433±10	345±9
y/x (-)	0	0.89	0.77	1	0.53	0.72	0.81	0.76	1.28	0.51	0.84	1.04	1.27	1.02	0.70	0.71	1.01	1.29
n (-)	0	25	48	48	17	1	1	1	1	1	33	17	1	1	33	17	33	48

Figure 4. Differences of the yield strength $R_{p0.2}$ of samples with artificial pits and the uncorroded aluminium alloy EN AW 2024-T3 with a yield strength of 350 MPa. The x-label shows the LSM measured average defect parameters and corresponding standard deviations.

As presented in figure 4, a large number of the investigated samples show a small reduction in yield strength of up to 5 MPa. For stationary loading applications, this reduction is compensated by the used safety factor during the dimensioning process. The yield strength of the uncorroded aluminium alloy EN AW 2024-T3 is 350 MPa. The strongest yield reduction of 14 MPa occurs for the samples with 48 defects, an aspect ratio of 1.29 and a depth of 225 µm. Only three samples show a yield strength reduction greater than 5 MPa. The pit depths for all three samples are greater than 225 µm, the widths in tensile direction are greater than 345 µm and the aspect ratios are greater than 0.7. Considering only these samples, the yield strength decreases if the aspect ratio *y*/*x* of the pits increases even if the pit depth decreases. Moreover, the yield strength decreases if the number of pits increases. Therefore, not only the penetration depths influences the yield strength reduction, but the aspect ratio and the number of pits seems to be the dominating factors when it comes to strength reduction after reaching the critical pitting corrosion parameters.

However, the differences in $R_{p0.2}$ are not large enough in this work to model the resulting yield strength in dependence on the defect parameters.

4. Conclusions

Electrochemical pitting corrosion was imitated using laser micro machining. The resulting uniaxial yield strength of the aluminium alloy EN AW-2024-T3 was investigated. It was observed that the hardness of the alloy is not significantly affected by the heat impact of the laser beam. The stress field around and inside the real and artificially produced pits are similar. Simple defect structures, e.g. conical frustums, show larger differences. Overall, it was shown that laser micro machining is a suitable technique to reproduce electrochemical pitting corrosion (excluding undercuts). In this work, a wide range of the investigated pitting corrosion states are within a uniaxial yield strength reduction of 5 MPa. A strong influence of pitting corrosion could be observed just for pits with a depth greater than 225 µm, a width in tensile direction greater than 345 µm and an aspect ratio of 0.7.

In further investigations, the number of tested samples with individual defect parameters could be raised. This would lead to more data for modelling the resulting yield strength in dependence of the defect parameters. After that, the constitutive relation for corroded materials could be applied on component parts in FE simulations.

Acknowledgments

Financial support was granted by the Deutsche Forschungsgemeinschaft (German Research Foundation) via the project LA 1274/36-1. The technical assistance of C. Gläser, K. Muhr, D. Spieler, H. Böhme and the numerical assistance of Mehadi Ziko is gratefully acknowledged.

References

[1] Campestrini P, van Westing E, van Rooijen H and de Wit J 2000 *Corros. Sci.* **42** 1853-61
[2] Strehblow H H 1984 *Mater. Corros.* **35** 437–48
[3] Blanc C and Mankowski G 1998 *Corros. Sci.* **40** 411–29
[4] Suter T and Alkire R C 2001 *J. Electrochem. Soc.* **148** B36–42
[5] Birbilis N and Buchheit R G 2005 *J. Electrochem. Soc.* **152** B140–51
[6] Obispo H, Murr L, Arrowood R and Trillo E 2000 *J. Mater. Sci.* **35** 3479-95
[7] Cerit M, Genel K and Eksi S 2009 *Eng. Fail. Anal.* **16** 2467–72
[8] Pidaparti R M and Rao A S 2008 *Corros. Sci.* **50** 1932–38
[9] Turnbull A, Wright L and Crocker L 2010 *Corros. Sci.* **52** 1492–98
[10] Sankaran K, Perez R and Jata K 2001 *Mater. Sci. Eng. A* **297** 223–29
[11] Wang Q, Kawagoishi N and Chen Q 2003 *Scripta Mater.* **49** 711–16
[12] Pantelakis S and Kermanidis A 2009 *Corrosion Control in the Aerospace Industry* 67 – 108
[13] Pantelakis S, Chamos A and Kermanidis A 2012 *Theor. Appl. Fract. Mec.* **57** 36–42
[14] Setsika D, Tserpes K and Pantelakis S 2015 *Int. J. Struct. Integ.* **6** 451–67
[15] Pantelakis S, Setsika D, Chamos A and Zervaki A 2016 *Int. J. Struct. Integ.* **7** 25–46
[16] van der Walde K, Brockenbrough J, Craig B and Hillberry B 2005 *Int. J. Fatigue* **27** 1509–18
[17] van der Walde K and Hillberry B 2008 *Int. J. Fatigue* **30** 106–18